Isı Bilimi ve Tekniği Dergisi, 40, 1, 177-194, 2020
J. of Thermal Science and Technology
©2020 TIBTD Printed in Turkey
ISSN 1300-3615

ENHANCEMENT OF HEAT TRANSFER BY HEAT PIPES WITH PIECEWISE UNIFORM LONGITUDINAL WICK PROFILES

Mehmed Akif PAKSOY * and Salih Özen ÜNVERDİ **
* TÜBİTAK BİLGEM BTE, 41400 Gebze, Kocaeli, makifpaksoy@live.com
** Gebze Technical University Department of Mechanical Engineering
41400 Gebze, Kocaeli, sunverdi@gtu.edu.tr

(Geliş Tarihi: 16.10.2019, Kabul Tarihi: 18.03.2020)

Abstract: An equation (29) is derived to calculate heat transfer rate of a heat pipe evaporator in terms of liquid pressure loss along and temperature difference across the wick and thermo-fluid properties, which shows that various wick profiles transfer same amount of heat under the constraints of pressure loss and temperature difference. It is proved by calculus of variations that among these profiles, wick weight is minimized in case of uniform wick thickness. Case studies are applied for a copper-water heat pipe with a wick of 0.5 porosity, $1.5\text{x}10^{-9}$ m^2 permeability, 8.65 mm outer radius and around 1.96 W/mK thermal conductivity. A case study shows that sum of the pressure losses of the liquid and vapor phases of the adiabatic region is minimized at a certain ratio of vapor core radius to wick outer radius. Finally, 1-D coupled flow and thermal analyses of the wick and vapor core of the heat pipe are performed for two types of designs with piecewise uniform wick thickness profiles which are proposed in this study. Under the constraint of constant total wick volume, heat transfer rate is plotted as function of wick thicknesses for each design. Without the wick volume constraint, increasing the adiabatic zone and condenser wick thicknesses while decreasing wick thickness of the evaporator enhances heat transfer rate up to 6.3%. On the other hand, increasing adiabatic zone wick thickness while decreasing that of the evaporator and condenser improves heat transfer rate up to 26.9% at capillary limit.
Keywords: Heat pipe, wick, optimization, wick thickness, wick profile, wick volume, wick weight, calculus of variations.

PARÇALI ÜNİFORM BOYLAMASINA FİTİL PROFİLLİ ISI BORULARI İLE ISI TRANSFERİNİN ARTTIRILMASI

Özet: Bir ısı borusu evaporatöründe ısı transferini fitildeki eksenel basınç kaybı ve radyal sıcaklık değişimi ile termo-fiziksel özelliklere bağlı olarak hesaplamak amacıyla bir bağıntı (29) çıkartılmış, basınç kaybı ve sıcaklık farkı kısıtları altında farklı fitil profillerinin aynı miktarda ısı transfer ettiği gösterilmiştir. Varyasyonlar hesabı ile fitil ağırlığının farklı fitil profilleri arasında sabit kalınlıkta olan için minimum olduğu ispatlanmıştır. Örnek çalışmalar 0.5 porozite, $1.5\text{x}10^{-9}$ m^2 geçirgenlik, 8.65 mm dış yarıçap ve yaklaşık 1.96 W/mK ısıl iletkenliğe sahip bir fitili olan bakır-su ısı borusu için gerçekleştirilmiştir. Bir örnek çalışmayla adyabatik bölgede, buhar akış yarıçapının fitil dış yarıçapına oranının belirli bir değerinde, sıvı ve buhar fazları basınç kayıpları toplamının minimum olduğu gösterilmiştir. Daha sonra, bu çalışmada önerilen bölgesel olarak sabit kalınlıkta iki farklı fitil tasarımı için ısı borusu fitil ve buhar kolonunun bir boyutlu bağlaşık akış ve ısıl analizleri gerçekleştirilmiştir. Sabit toplam fitil hacmi kısıtı altında, her iki tasarım için ısı transferi bölgesel fitil kalınlıklarının fonksiyonu olarak çizdirilmiştir. Fitil hacmi kısıtı kaldırıldığında, adyabatik bölge ve kondenser fitil kalınlıkları arttırılıp, evaporatör fitil kalınlığı azaltıldığında ısı transferi %6.3'e kadar artmıştır. Öte yandan, adyabatik bölge fitil kalınlığı arttırılıp, evaporatör ve kondenser fitil kalınlığı azaltıldığında kapiler limitte ısı transferi %26.9'a kadar artmıştır.
Anahtar kelimeler: Isı borusu, fitil, optimizasyon, fitil kalınlığı, fitil profili, fitil hacmi, fitil ağırlığı, varyasyonlar hesabı.

NOMENCLATURE

A	Cross sectional area [m^2]	T_p	Wick outer surface temperature [K]
a	Constant defined in Eq. (19) [m]	T_v	Vapor temperature [K]
b, c	Constants defined in Eq. (24) [-], [m]	t	Wick thickness [m]
C	Thermo-physical properties group, defined in Eq. (31) [W m^{-1} $Pa^{-1/2}$ $K^{-1/2}$]	V	Bulk volume [m^3]
C_1	Thermo-physical properties group, defined in Eq. (49) [$K^{1/2}$ $Pa^{-1/2}$]	**Greek Symbols**	
D	Constant defined in Eq. (34) [-]	ΔP	Pressure loss [Pa]

f	Darcy friction factor [-]
$f(x)$	Function defining wick thickness profile [m]
h_{fg}	Latent heat of evaporation of working fluid [J kg^{-1}]
K	Permeability of the wick [m^2]
k	Thermal conductivity [W m^{-1} K^{-1}]
k_{eff}	Effective wick thermal conductivity [W m^{-1} K^{-1}]
L	Length [m]
$\dot{m}$	Mass flow rate [kg s^{-1}]
Q	Heat transfer rate [W]
q''	Heat flux [W m^{-2}]
R	Radial thermal resistance [K W^{-1}]
r	Wick outer radius [m]
r_{cap}	Capillary radius [m]
T	Temperature [K]
T_c	Condenser wick outer surface temperature [K]
T_h	Evaporator wick outer surface temperature [K]
ΔT	Temperature difference between the pipe side and vapor side of the wick [K]
ΔT_v	Vapor temperature drop [K]
η	Dummy variable for "x"
μ	Dynamic viscosity [Pa s]
ρ	Density [kg m^{-3}]
φ	Wick porosity [-]
σ	Surface tension [N m^{-1}]

Subscripts

a	Adiabatic zone
c	Condenser
$diff$	Differential element
e	Evaporator
eff	Effective
l	Liquid
p	Pipe
v	Vapor
w	Wick

INTRODUCTION

Heat pipes are becoming increasingly popular in various applications because of their high efficiencies, high heat removal rates, small sizes, compact designs and robust performance (Lin and Wong, 2013; Zohuri, 2016). Number of experimental and mathematical modeling studies on various types of heat pipes are increasing in conformity with the ever-growing application areas of heat pipes. Some researchers focused their attention on very detailed thermo-fluid models and obtained very good agreement between experimental and numerical results (Ranjan et al., 2009; Huang and Chen, 2017; Ranjan et al., 2011). On the other hand, there are many experimental studies which try to understand heat pipes' thermo-fluid characteristics and various limits, and to enhance their thermal performances (Wang et al., 2014; Wong et al., 2017; Deng et al., 2013).

Mono-porous sintered powder wick is one of the most common wick types used in heat pipes. Yet, the effect of various wick parameters like pore structure, particle size and wick thickness on thermal performance of a heat pipe are not investigated comprehensively. Weibel et al., 2010, showed that for a given wick thickness, there is a tradeoff between increased area for heat transfer and increased resistance to vapor flow out of the wick, as the particle size changes. Therefore, an optimum particle size exists which minimizes the thermal resistance. However further study is required since particle size is not only related to thermal resistance, but also to capillary head which is a limiting factor for overall heat pipe performance (Lin and Wong, 2013).

In their study, Hong et.al., 2013. experimentally showed that there exists an optimum wick thickness for which effective heat transfer coefficient is maximized when particle size and type (or porosity) of the wick and other parameters of a heat pipe are fixed. However, in the study it is also noted that experimentally found optimum wick thickness may not be the real optimum since experimental data can be obtained only for discrete wick thickness values.

There are numerous studies suggesting better wick designs. Siddiqui and Kaya, 2016, designed and thermally analyzed an arterial type heat pipe with mesh wick. The study is focused on venting hole diameter and distance between venting holes. They optimized these two geometric parameters considering pressure loss and bubble blockage. Critical venting hole diameter is found by developing a meniscus coalescence criterion which can be defined in terms of the geometrical parameters. Choosing lowest possible hole diameter that satisfies meniscus coalescence criterion yields lowest possible pressure loss. Furthermore, they optimized the distance between venting holes where smaller distance increases number of holes and decreases the clearance time of arteries blocked by bubbles but increases the pressure loss, thereby reducing heat transfer limit of the heat pipe. On the other hand bigger distance between holes increases the clearance time and decreases the pressure loss hence increasing heat transfer limit.

On the modeling side, Zuo and Faghri, 1998, successfully simulated the transient behavior of a heat pipe. Their model is based on a thermal network which results in a set of linear, first order ordinary differential equations, whose solution gives information about the transient thermo-fluid behavior of the heat pipe. Their results were fairly accurate when compared with experimental data. Their findings are also compared with those obtained from both a two-dimensional numerical model and a lumped model and it can be concluded that there are

slight deviations in transient vapor temperatures, but it is observed that the differences among the results are minimal at steady state. Tournier and El-Genk, 1994, developed a two-dimensional numerical model suitable for transient analysis of a heat pipe. Their model involved calculation of radius of curvature of the liquid meniscus which forms at the liquid-vapor interface. Calculated transient and steady-state temperatures were in well agreement with experiments. Kaya and Goldak, 2007, presented a three-dimensional finite element model for simulations of heat pipes at steady state. They showed that vapor flow field remains nearly symmetrical about the heat pipe axis even for a non-uniform heat load. Mwaba et al., 2006, suggested a composite wick which is made from coarse mesh copper screen in condenser and adiabatic region and sintered fine copper powder in evaporator. This design results in lower pressure loss in liquid phase while increasing allowable capillary head in comparison to using sintered wick through the entire heat pipe. They solved the thermo-fluid problem by a commercial CFD software where phase change at the liquid-vapor interface is modeled with momentum and energy sources and sinks. Simulation results showed that wick structure affects heat pipe performance significantly and suggested composite wick can enhance heat pipe performance up to a factor of two.

Most of the modeling studies in the literature and described above tried to model the operational characteristics of heat pipes. One of the few exceptions is the study of Nishikawara and Nagano, 2017. In their study they incorporated the effect of geometrical parameters (i.e. number and size of axial and circumferential grooves) of the wick to evaporator heat transfer coefficient by relating the length of three-phase contact line to groove numbers. They investigated the effect of increasing the length of three-phase contact line and showed that heat transfer coefficient increases up to a point and then starts to decrease because of large distribution of saturation temperature as a result of bigger pressure loss in the grooves. Another study on heat pipe optimization is by Kiseev et al., 2010, where they investigated the effect of capillary structure on heat transfer. They proposed a methodology to calculate capillary structure's effective pores radius which maximizes heat transfer for loop heat pipes.

In this study, a 1-D thermo-fluid model of a conventional heat pipe is developed to investigate the effect of wick profile (i.e. thickness variation) along the heat pipe on heat transfer. To clarify, in Figure 1 (a) longitudinal section of a conventional cylindrical heat pipe with constant wick thickness is presented. Increasing wick thickness profiles along the evaporator which are linear, non-linear (i.e. curved) concave up and concave down are shown in Figure 1 (b), (c), and (d), respectively, while maintaining constant wick thickness along the adiabatic zone and condenser. First, the optimum wick thickness profile along the evaporator that maximizes heat transfer rate is searched under the constraint of a specified pressure loss along the wick. However, it is found that under the constraint of pressure loss, any evaporator wick profile transfers same amount of heat. So, from this perspective there is not an optimum solution. Then, the optimum wick thickness profile along the evaporator is searched for which minimum evaporator weight is achieved under the constraint of a specified pressure loss along the wick, and by calculus of variations it is found that uniform wick thickness is the solution. The study is extended to the condenser and adiabatic zone to obtain the optimum wick thickness profile for each region. Finally, for two types of designs proposed in this study, under the constraint of overall pressure loss in heat pipe cycle which is imposed by capillary head, piecewise uniform wick thicknesses of evaporator, adiabatic zone and condenser that maximize heat transfer rate are calculated.

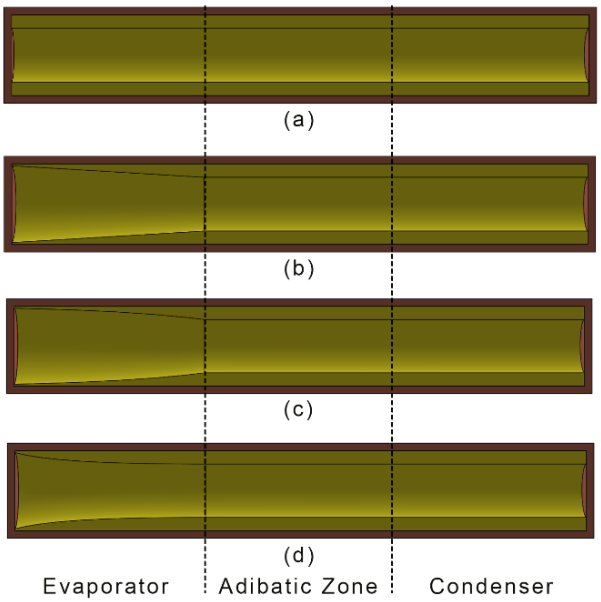

Figure 1. Wick thickness profiles for the longitudinal section of a heat pipe (a: Uniform, b: Linearly increasing, c: Concave up, increasing, d: Concave down, increasing profiles for the evaporator).

THEORY

An analytical model for calculating steady-state heat transfer rate and pressure loss through the evaporator wick of a heat pipe is developed. Then heat transfer rate and pressure loss through the evaporator wick is related using the developed analytical models. Calculus of variations is applied to the developed models in order to minimize volume, therefore weight, of the evaporator wick. Developed models and relations are extended to the condenser wick. Furthermore, steady-state pressure losses are modeled analytically in liquid and gas phases, where both laminar and turbulent regimes are considered for gas flow, of the adiabatic region.

Evaporator Analytical Model

In Figure 2 modeled region, i.e. evaporator wick, is presented with some definitions. Evaporator length, which is measured in x-axis direction, and wick's outer

radius are denoted by L and r, respectively. Evaporator thickness profile is represented with function f(x). T_v is vapor temperature and T_p is the temperature of the wick outer surface which is in contact with heat pipe wall. It is assumed that T_p and T_v are constant throughout the x direction. Therefore, axial heat transfer, in x direction, is neglected since T_p and T_v are assumed to be uniform in axial direction.

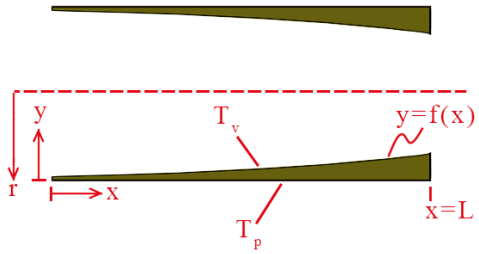

Figure 2. Modeled evaporator wick and notation.

The thermal model is based on conduction through the wick in radial direction using the effective heat transfer coefficient which is defined as (Zuo and Faghri, 1998)

$$k_{eff} = \frac{k_l[(k_l + k_w) - (1-\varphi)(k_l - k_w)]}{[(k_l + k_w) + (1-\varphi)(k_l - k_w)]} \quad (1)$$

in terms of liquid thermal conductivity, k_l, wick material thermal conductivity, k_w, and porosity, φ. Definition of effective heat transfer coefficient, k_{eff}, as a parameter facilitates formulation of the problem in terms of wick thickness, f(x).

Assuming a linear temperature profile in radial direction in the wick, heat transfer rate in y direction for a cylindrical differential element with height dx can be expressed as

$$dQ = k_{eff}\frac{T_p - T_v}{f(x)}dx \cdot 2\pi r \quad (2)$$

Therefore, heat transfer rate throughout the evaporator can be calculated as

$$Q = \int_0^L k_{eff}\frac{T_p - T_v}{f(x)}dx \cdot 2\pi r \quad (3)$$

This expression can be simplified by assuming that the factors k_{eff}, $\Delta T = T_p - T_v$ and r are constant and can be taken out of the integral, which results in

$$Q = 2\pi r k_{eff}\Delta T \int_0^L \frac{dx}{f(x)} \quad (4)$$

According to Darcy's Law, pressure loss through a differential element dx in axial direction can be calculated as

$$dP = \frac{\mu_l \dot{m}_l(x)}{\rho_l A_w(x) K}dx \quad (5)$$

where, $\dot{m}_l$ is the liquid mass flow rate in the wick in negative x direction. Considering the integral control volume around the wick of the evaporator shown in Figure 3, mass flow rate entering the volume in liquid phase and leaving the volume in vapor phase should be equal at steady state.

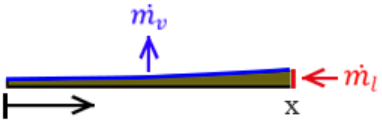

Figure 3. Mass flow rate balance for an integral control volume around the wick of the evaporator.

As the heat transferred to the evaporator from the surroundings should be absorbed by the liquid in the wick as it evaporates at steady state, mass flow rate of the working fluid can be expressed as

$$\dot{m}_l = \dot{m}_v = \frac{2\pi r k_{eff}\Delta T \int_0^x \frac{d\eta}{f(\eta)}}{h_{fg}} \quad (6)$$

where, h_{fg} is the latent heat of evaporation of the fluid. Inserting the mass flow rate (6) into the pressure drop Eq. (5) and integrating along the evaporator results in liquid pressure loss along the evaporator wick as

$$\Delta P = \int_0^L \frac{\mu_l 2\pi r k_{eff}\Delta T \int_0^x \frac{d\eta}{f(\eta)}}{\rho_l A_w(x) K h_{fg}}dx \quad (7)$$

Since heat pipe outer radius is much bigger than the thickness of the wick, i.e. r ≫f(x), cross-sectional area of the wick at axial position x can be approximately calculated as

$$A_w(x) = 2\pi r f(x) \quad (8)$$

Inserting the wick cross-sectional area in Eq. (7), the liquid pressure loss along the evaporator is calculated as

$$\Delta P = \int_0^L \frac{\mu_l k_{eff}\Delta T \int_0^x \frac{d\eta}{f(\eta)}}{\rho_l K h_{fg} f(x)}dx \quad (9)$$

and taking constant factors μ_l, k_{eff}, ΔT, ρ_l, K, h_{fg} out of the integral sign results in

$$\Delta P = \frac{\mu_l k_{eff}\Delta T}{\rho_l K h_{fg}} \int_0^L \frac{\int_0^x \frac{d\eta}{f(\eta)}}{f(x)}dx \quad (10)$$

Relation Between Heat Transfer Rate and Pressure Loss of the Evaporator

Eqs. (4) and (10) are evaporator heat transfer rate and liquid pressure loss along the wick of the evaporator, respectively. Optimum wick profile f(x) can be calculated by either keeping pressure loss constant and maximizing heat transfer rate or by keeping heat transfer rate constant and minimizing pressure loss. In this study, maximization of heat transfer rate throughout the evaporator while keeping the pressure loss along the wick constant, as the wick profile changes, is considered.

First define g(x) as

$$g(x) = \int_0^x \frac{d\eta}{f(\eta)} \quad (11)$$

Taking derivative of both sides with respect to x results in

$$g'(x) = \frac{1}{f(x)} \tag{12}$$

Expressing Eq. (4) in terms of g(L) and Eq. (10) in terms of g(x) and g'(x)results in

$$Q = 2\pi r k_{eff} \Delta T g(L) \tag{13}$$

and

$$\Delta P = \frac{\mu_l k_{eff} \Delta T}{\rho_l K h_{fg}} \int_0^L g(x) g'(x) dx \tag{14}$$

respectively. It is required to select a g(x) that satisfies Eq. (14) for a given ΔP and maximize evaporator heat transfer rate which is given by Eq. (13). Solution of Eq. (14) is

$$\Delta P = \frac{\mu_l k_{eff} \Delta T}{\rho_l K h_{fg}} \left| {}_0^L \frac{g(x)^2}{2} \right. \tag{15}$$

so that,

$$\Delta P = \frac{\mu_l k_{eff} \Delta T}{\rho_l K h_{fg}} \left[\frac{g(L)^2}{2} - \frac{g(0)^2}{2} \right] \tag{16}$$

It can be seen from Eq. (11) that g(0)=0, so pressure drop given by Eq. (16) becomes

$$\Delta P = \frac{\mu_l k_{eff} \Delta T}{2\rho_l K h_{fg}} g(L)^2 \tag{17}$$

Combining Eqs. (13) and (17) evaporator heat transfer rate can be calculated as

$$Q = 2\pi r \sqrt{\frac{2\rho_l K h_{fg} k_{eff} \Delta T \Delta P}{\mu_l}} \tag{18}$$

Eqs. (11) and (17) state that same pressure loss can be obtained with various wick thickness profiles, therefore according to Eq. (18), same heat transfer rate may be achieved with many wick thickness profiles satisfying Eq. (17) with constant g(L) for the prescribed pressure loss.

For example, considering a wick of constant thickness as in Figure 1 (a)

$$f(x) = a \tag{19}$$

Inserting this in Eq. (11) and integrating gives

$$g(L) = \int_0^L \frac{dx}{a} = \left| {}_0^L \frac{x}{a} \right. = \frac{L}{a} \tag{20}$$

Then, inserting Eq. (20) in Eq. (17) results in pressure loss for the case of uniform wick thickness as

$$\Delta P = \frac{\mu_l k_{eff} \Delta T}{2\rho_l K h_{fg}} \frac{L^2}{a^2} \tag{21}$$

from which wick thickness, a, is obtained in terms of evaporator length, permeability of the wick, thermo-fluid properties of the fluid, and pressure and temperature differentials as

$$a = \sqrt{\frac{\mu_l k_{eff} \Delta T L^2}{\Delta P 2\rho_l K h_{fg}}} \tag{22}$$

Heat transfer rate for constant wick thickness that satisfies a given pressure loss can be obtained by inserting (20) and (22) in Eq. (13) as

$$Q = 2\pi r \sqrt{\frac{2\rho_l K h_{fg} k_{eff} \Delta T \Delta P}{\mu_l}} \tag{23}$$

This can be compared with linearly increasing wick profile, Figure 1 (b), where b and c are not known

$$f(x) = bx + c \tag{24}$$

Writing the linear profile in Eq. (11) and integrating gives

$$g(L) = \frac{1}{b} In\left(\frac{bL + c}{c}\right) \tag{25}$$

Inserting calculated g(L) in Eq. (17) gives

$$\Delta P = \frac{\mu_l k_{eff} \Delta T}{2\rho_l K h_{fg}} \left[\frac{1}{b} In\left(\frac{bL + c}{c}\right)\right]^2 \tag{26}$$

Different b and c combinations can satisfy the above equation for a given pressure loss, ΔP. Eq. (17) can be rewritten to express g(L) in terms of ΔP which is given above, as

$$g(L) = \sqrt{\frac{\Delta P 2\rho_l K h_{fg}}{\mu_l k_{eff} \Delta T}} = \frac{1}{b} In\left(\frac{bL + c}{c}\right) \tag{27}$$

Inserting g(L) in Eq. (13) gives the heat transfer rate for linear wick profile that satisfies the pressure loss criterion

$$Q = 2\pi r \sqrt{\frac{2\rho_l K h_{fg} k_{eff} \Delta T \Delta P}{\mu_l}} \tag{28}$$

Comparing Eqs. (23) and (28), it is seen that evaporator heat transfer rate, Q, for any wick profile can be calculated with Eq. (18) in terms of ΔT and ΔP.

By dividing both sides of Eq. (28) with $\sqrt{\Delta P \Delta T}$ and wick outer area, an equation is obtained where right-hand side is a group of constants which is

$$\frac{Q}{2\pi r L \sqrt{\Delta P \Delta T}} = \sqrt{\frac{2\rho_l K h_{fg} k_{eff}}{\mu_l L^2}} \tag{29}$$

Eq. (29) can be simplified as follows:

$$q'' = \frac{Q}{2\pi r L} \tag{30}$$

$$C = \sqrt{\frac{2\rho_l K h_{fg} k_{eff}}{\mu_l}} \tag{31}$$

$$q'' = C \sqrt{\frac{\Delta P}{L} \times \frac{\Delta T}{L}} \tag{32}$$

Eq. (32) relates heat flux to pressure loss along and temperature difference across the evaporator wick. For an evaporator with a chosen wick profile operating at maximum allowable evaporator pressure loss, if the

temperature difference increases dry out occurs as liquid cannot be fed to the tip of the evaporator so that the heat transfer rate cannot be further increased. To increase the heat transfer rate, the entire wick of the evaporator must be wetted which is only possible by increasing its thickness. On the other hand, if the temperature difference decreases, so does the heat flux and therefore pressure loss according to Eq. (32).

Constrained Optimization of the Evaporator Weight

In the previous section it is shown that there is a functional relation, Eq. (29), between evaporator heat transfer rate and liquid phase pressure loss along the wick of the evaporator and temperature difference across the wick of a heat pipe even though wick thickness profile may change. However, the amount of material used for different wick thickness profiles are not the same and there may be an optimum profile for which minimum amount of wick material is used. For a chosen wick material and micro-structure, mass of the evaporator wick is proportional to bulk volume of it which can be expressed based on Eq. (8) as

$$V_w(L) = \int_0^L 2\pi r f(x) dx \tag{33}$$

For a specified heat transfer rate Q, and for any wick thickness profile f(x) that satisfies a specified liquid phase pressure loss ΔP along the wick of evaporator, from Eqs. (17) and (18) one can write

$$g(L) = \int_0^L \frac{dx}{f(x)} = \frac{4\pi r \rho_l K h_{fg}}{\mu_l} \frac{\Delta P}{Q} = D \tag{34}$$

where D is a constant. Thus, minimization of the evaporator wick volume $V_w(L)$ which is given by Eq. (33) under the constraint (34), which expresses a relation between the chosen liquid pressure loss, ΔP, along the wick and wick thickness profile, f(x), is to be considered. This is an isoperimetric problem in calculus of variations (Lemons, 1997; Gelfand and Fomin, 1963), where wick thickness profile function, f(x), is to be found that minimizes the wick volume functional, $V(f)= \int_0^L F(f)dx$, where $F(f)=2\pi rf$, while functional $g(f)= \int_0^L G(f)dx$, where $G(f)=1/f$, satisfying the subsidiary condition or constraint $g(f)=D$ is imposed on admissible curves f(x) as well as two boundary conditions f(0)=A and f(L)=B.

According to the theorem for a variational problem with a subsidiary condition, f(x), satisfies the differential equation

$$F_f - \frac{d}{dx} F_{f'} - \lambda \left[G_f - \frac{d}{dx} G_{f'} \right] = 0 \tag{35}$$

where, F=F(x,f,f') and G=G(x,f,f') (Gelfand and Fomin, 1963). In our special case, second and fourth terms of the differential equation drop out, because $F_{f'} = G_{f'} = 0$. Inserting $F_f = 2\pi r$ and $G_f = -1/f^2$ following algebraic equation is obtained

$$2\pi r - \frac{\lambda}{f^2} = 0 \tag{36}$$

Therefore, wick thickness should be a positive constant throughout the evaporator. Inserting this constant wick thickness into Eq. (34) and performing integration results in

$$\frac{f}{L} = \sqrt{\frac{\mu_l k_{eff}}{2\rho_l K h_{fg}} \frac{\Delta T}{\Delta P}} = \frac{\mu_l}{4\pi r \rho_l K h_{fg}} \frac{Q}{\Delta P} \tag{37}$$

which is the result obtained earlier for a uniform wick thickness in Eq. (22). We conclude that the wick thickness at two endpoints of the evaporator should be equal, i.e. f(0)=f(L), or A=B, in order to have a solution to the minimum mass of the wick problem for specified heat transfer rate, Q, and liquid phase pressure loss, ΔP.

This result shows that out of different wick profiles with the same pressure loss and heat transfer rate at the evaporator, the lowest wick mass is obtained with uniform wick thickness, which is given in terms of the length of the evaporator, outer radius and permeability of the wick, thermo-fluid properties of the working fluid, heat transfer rate and pressure loss of liquid phase inside the wick along the evaporator in Eq. (37).

Extending Developed Model to the Condenser

The model developed for the evaporator can be extended to the condenser since the analytical expressions of the physical mechanisms are similar, except that mass and heat fluxes are in opposite directions. Modeled condenser region of the heat pipe is presented in Figure 4.

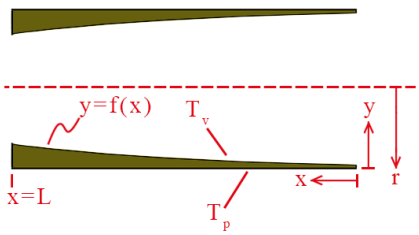

Figure 4. Modeled condenser wick of the heat pipe and the notation.

Heat transfer rate in -y direction for a differential ring element with outer radius, r, thickness, f(x), and height, dx, is

$$dQ = k_{eff} \frac{T_v - T_p}{f(x)} dx \cdot 2\pi r \tag{38}$$

Hence, heat transfer rate throughout the condenser with length, L, is calculated as

$$Q = \int_0^L k_{eff} \frac{T_v - T_p}{f(x)} dx \cdot 2\pi r \tag{39}$$

This expression can be simplified by taking constant quantities out of the integral sign

$$Q = 2\pi r k_{eff} \Delta T \int_0^L \frac{dx}{f(x)} \tag{40}$$

where $\Delta T=T_v-T_p$. Expression given above is the same as the heat transfer rate of the evaporator given in Eq. (4)

except that heat transfer is in opposite direction to that of the evaporator.

Pressure loss along the wick of the evaporator and adiabatic zone and condenser can be expressed by Darcy's Law given in Eq. (5). Mass flow rates through the control surfaces of the integral control volume enclosing the wick of the condenser are shown in Figure 5, where mass flow rate entering the control volume from the vapor phase and leaving the control volume in the liquid phase should be equal in steady state.

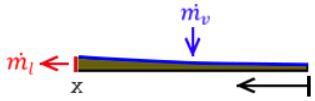

Figure 5. Mass flow rates for the integral control volume enclosing the wick of the condenser.

As the heat rejection rate from the condenser to the surroundings is equal to the mass flow rate times latent heat of condensation of the working fluid at steady state, mass flow rate of the working fluid can be expressed as

$$\dot{m}_l = \dot{m}_v = \frac{2\pi r k_{eff} \Delta T \int_0^x \frac{d\eta}{f(\eta)}}{h_{fg}} \tag{41}$$

Hence, inserting mass flow rate given by Eq. (41) into Darcy's Law, Eq. (5), results in the pressure loss along the condenser wick

$$\Delta P = \int_0^L \frac{\mu_l 2\pi r k_{eff} \Delta T \int_0^x \frac{d\eta}{f(\eta)}}{\rho_l A_w(x) K h_{fg}} dx \tag{42}$$

Assuming the heat pipe radius is much bigger than the wick thickness, i.e. r >> f(x), the cross-sectional area of the wick, $A_w(x)$, can be calculated by Eq. (8). Inserting the cross-sectional area in Eq. (42) and taking constant quantities out of the integral sign, pressure loss along the wick becomes:

$$\Delta P = \frac{\mu_l k_{eff} \Delta T}{\rho_l K h_{fg}} \int_0^L \frac{\int_0^x \frac{d\eta}{f(\eta)}}{f(x)} dx \tag{43}$$

Mass of the condenser wick is proportional to the bulk volume of the wick which is equal to the integral of the cross-sectional area along the length of the condenser as given in Eq. (33).

Pressure loss expressions for the condenser, Eq. (43), and evaporator, Eq. (10), are identical, therefore the relation, Eq. (18), between heat transfer rate, Q, pressure loss, ΔP, and temperature difference, ΔT, derived for evaporator can be applied to condenser as well. Finally, among these wick profiles, lowest wick mass is attained when the wick thickness is uniform along the condenser which may be calculated by Eq. (37).

Reducing Pressure Losses in the Adiabatic Zone

Consideration of the entire wick in a heat pipe including the evaporator, adiabatic zone and the condenser is necessary to apply the findings of this study. Modeling and optimization of the adiabatic section is simpler in comparison to evaporator and condenser since heat transfer and phase change phenomena can be neglected so only pressure loss needs to be considered. For the adiabatic zone, uniform wick thickness results in the minimum pressure loss among various wick profiles, because excessive pressure losses due to constriction and expansion are avoided. A case study comparing pressure losses for uniform and non-uniform wick profiles in the adiabatic zone, for both laminar and turbulent vapor flows, is presented in the appendix.

The modeled adiabatic region is shown in Figure 6. For the adiabatic region, mass flow rate of both phases should be equal according to conservation of mass principle at steady state

$$\dot{m} = \dot{m}_l = \dot{m}_v \tag{44}$$

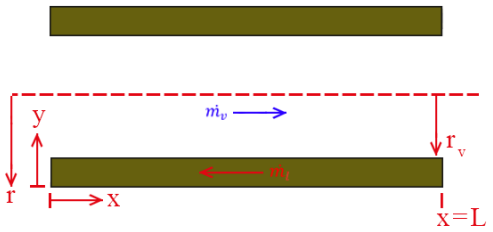

Figure 6. Modeled adiabatic zone and notation.

Pressure loss of vapor flowing along the axis of the heat pipe (vapor column) can be calculated by Poiseuille-Hagen and Darcy-Weisbach formulas for fully developed laminar and turbulent flows in a tube, respectively. On the other hand, pressure loss of liquid flowing along the porous wick of the adiabatic zone can be calculated by Darcy's law as in the case of evaporator and condenser. If the vapor flow is laminar, sum of the pressure losses in vapor and liquid phases along the length of the adiabatic zone, L_a, is

$$\Delta P_a = \frac{8\mu_v L_a \dot{m}}{\pi \rho_v r_v^4} + \frac{\mu_l \dot{m}}{\pi (r^2 - r_v^2) \rho_l K} L_a \tag{45}$$

whereas for turbulent vapor flow, it becomes

$$\Delta P_a = f \frac{L_a}{4} \frac{\dot{m}^2}{\pi^2 r_v^5 \rho_v} + \frac{\mu_l \dot{m}}{\pi (r^2 - r_v^2) \rho_l K} L_a \tag{46}$$

Adiabatic zone pressure loss curves for liquid flow in the porous wick and for vapor flow as well as their sum calculated by Eqs. (45) and (46) are plotted in Figure 7 as functions of ratio of vapor column radius to wick outer radius r_v/r while keeping wick outer radius, r, constant. Note that, Figure 7 is plotted for typical parameters of a conventional water-copper heat pipe existing in the literature which are given in Table 1 (Tournier and El-Genk, 1994), while changing r_v/r.

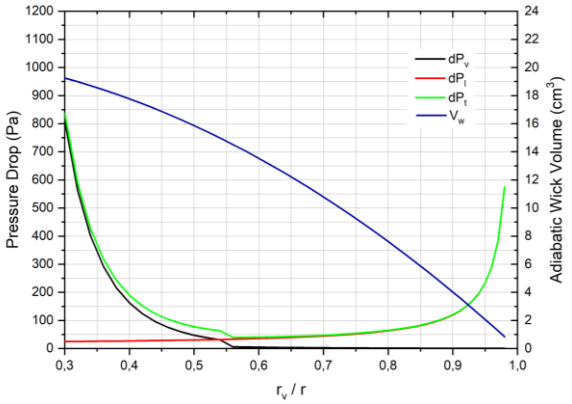

Figure 7. Pressure losses vapor in the adiabatic zone of the heat pipe as functions of vapor column radius to wick outer radius ratio, r_v/r (dP_l: liquid pressure loss, dP_v: vapor pressure loss, dP_t: total pressure loss, V_w: wick bulk volume).

Table 1. Typical water-copper heat pipe parameters for case studies.

Parameter	Value	Unit
L_e	600	mm
L_a	90	mm
L_c	200	mm
r	8.65	mm
r_v	7.90	mm
r_{cap}	54	μm
φ	0.5	%
K	1.5×10^{-9}	m^2
$\dot{m}$	0.188	gr/s

In Figure 7, at small values of r_v/r vapor flow is turbulent and pressure loss of vapor column is greater than that of the liquid flow in the porous wick. Around $r_v/r = 0.55$ vapor flow becomes laminar and pressure loss of liquid exceeds that of the vapor henceforth, i.e. for bigger values of r_v/r. For values of r_v/r greater than 0.9 a rapid increase in liquid phase pressure loss is observed. It is known from the literature that in most applications vapor pressure loss is less than that of the liquid in the wick (Tournier and El-Genk, 1994; Zhu and Vafai, 1999). This is because of selected r_v/r ratios in practice being above the threshold value given above, which adversely affects the performance of a heat pipe, for example for the typical heat pipe considered above $r_v/r = 0.91$.

Model Validation

A 1-D model is built using the Eq. (4) and (40) for heat transfer rate and Eq. (45) and (46) for liquid and vapor pressure losses. Details of the 1-D model are presented under section "1-D Analysis of Flow and Heat Transfer for a Heat Pipe". Developed models are validated with the experimental and numerical studies from the literature, and the results are presented in Table 2. Validation studies are carried out by using wick thermo-physical properties and wick outer surface temperature values obtained from the related studies as inputs while heat transfer rates and pressure losses are the outputs of the model (Tournier and El-Genk, 1994; Schmalhofer and Faghri, 1992; El-Genk and Huang, 1993). Good agreement between heat transfer rates are observed where deviations between the predictions of the present model and the measurements are less than 5%. On the other hand, the difference between the pressure losses calculated by the present model and the numerical model of Tournier and El-Genk, 1994, is around 10%. Deviations among the present 1-D model predictions and those of more sophisticated numerical simulations and experimental findings are reasonable since some assumptions and simplifications have been done for the present model to be analytically solvable.

Table 2. Heat transfer rates and pressure losses.

Case	Parameter	Unit	Present Model	Tournier and El-Genk, 1994		Schmalhofer and Faghri, 1992	El-Genk and Huang, 1993
				exp.	num.	exp.	exp.
#1	Q	W	432	443	455	-	-
#2			144	-	-	150	-
#3			547	-	-	-	570
#1	ΔP	Pa	707	-	769	-	-
#2			286	-	-	-	-
#3			920	-	-	-	-

RESULTS AND DISCUSSION

Various Evaporator Wick Thickness Profiles

Heat pipe evaporators for which fundamental geometric and physical parameters are presented in Table 1 operating under typical conditions are analyzed by the developed analytical models. In the analyses, temperature difference over the wick thickness, ΔT, is assumed to be 5.51 K as used in the study of Tournier and El-Genk, 1994, which is a typical operating value. Effective wick thermal conductivity, k_{eff}, is calculated as 1.93 W/mK by Eq. (1). Functions of different wick thickness profiles studied for the evaporator are given in Table 3. Heat transfer rates, pressure losses and wick volumes presented in Table 3 are calculated by Eqs. (4), (7) and (33), respectively. Heat transfer rates and corresponding pressure losses are found to be equal for diversity of evaporator wick thickness profiles considered where slight differences in heat transfer rates and corresponding pressure losses are due to round-off errors. It should be noted that for wick profiles presented g(L) is constant since it is a pre-requisite for constant pressure loss which also results in constant heat transfer rate as deduced from Eqs. (17) and (18).

Table 3. Functions defining different wick profiles over evaporator.

Profile No	Wick profile (mm)	Value of constants	Q (W)	ΔP (Pa)	Wick volume (cm^3)
1	$y = c$	c=0.75	463.57	416.58	24.46
2	$y = bx + c$	b=3.326, c=0.15	463.53	416.50	37.43
3		b=2.024, c=0.30	463.51	416.47	29.58
4		b=1.184, c=0.45	463.61	416.64	26.26
5	$y = ax^2 + bx + c$	a=21.36, b=0 , c=0.15	463.59	416.61	88.48
6		a=13.21, b=1 , c=0.15	463.60	416.63	66.37
7		a=0.555, b=1 , c=0.45	463.60	416.62	26.63
8	$y = ax^b + c$	a=1.363, b=0.50, c= 0.15	463.59	416.62	27.84
9		a=2.119, b=0.75, c=0.15	463.59	416.61	31.81
10	$y = -ax^2 + bx + c$	a= 2, b= 3.816, c= 0.15	463.60	416.62	34.40

Reference uniform wick with 0.75 mm thickness and linearly increasing wick profiles (profiles 2 to 4) for which pressure loss in axial direction and resulting heat transfer rate is the same are plotted in Figure 8 over evaporator length. As can be seen from the figure, as the slope increases, wick thickness at the tip of the evaporator, x=0 m, decreases, while it increases at the end, x=0.6 m. It is also noted that as the slope decreases volume occupied by the wick decreases reducing wick material usage and allowing more space for vapor flow.

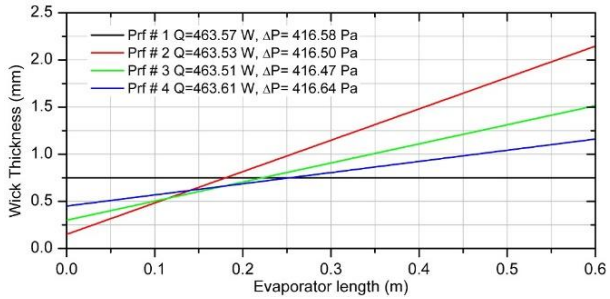

Figure 8. Linearly increasing wick profiles over evaporator.

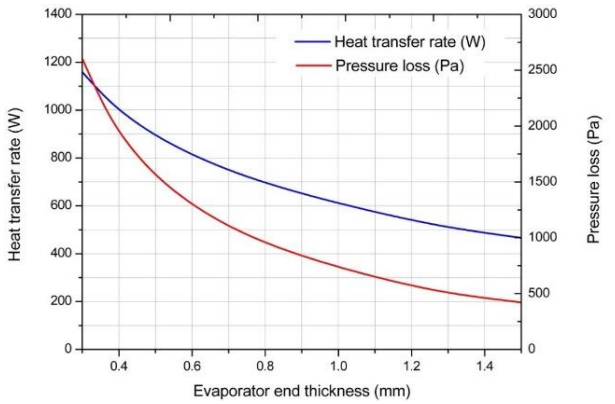

Figure 9. Change of heat transfer rate and pressure loss by evaporator end thickness.

Heat transfer rate and pressure loss along the evaporator are plotted in Figure 9, for 0.3 mm wick thickness at the tip, x=0 m, as the slope of the wick is increased which results in wick thickness at evaporator end, x= 0.6 m, change from 0.3 mm to 1.5 mm. Pressure loss and heat transfer rate both decrease with increasing slope of the wick profile. On the other hand, wick volume increases as heat transfer rate decreases in this case (Figure 10).

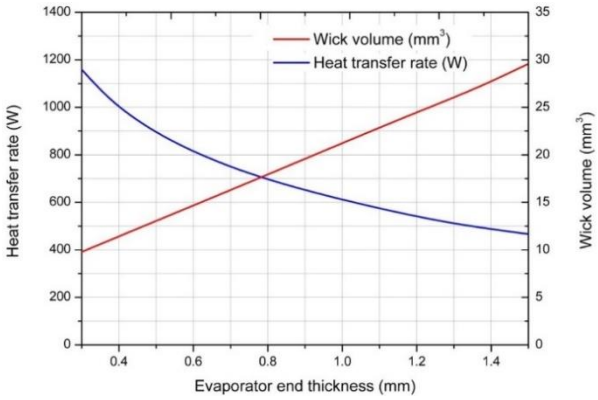

Figure 10. Change of heat transfer rate and wick volume by evaporator end thickness.

Parabolic wick thickness profiles which result in the same axial pressure loss and heat transfer rate given in Table 3 are plotted in Figure 11. As the wick thickness at the tip of the evaporator is decreased significantly below the uniform thickness, e.g. parabolic wick Profile # 5 in Figure 11, thickness at evaporator end, x=0.6 m, approaches to the pipe centerline to compensate the excessive pressure losses nearby the tip. Wick volume increases up to 360% in comparison to reference uniform wick profile where still pressure loss and heat transfer rate are the same. Increased wick thickness at evaporator end allows keeping fluid velocity thus pressure loss lower even though fluid flow rate is the highest at evaporator end. On the other hand, increased wick thickness decreases heat transfer rate locally, thereby balancing excessive heat transfer near the tip. The increased sensitivity of heat transfer rate and pressure losses to wick thickness as the thickness gets smaller can also be deduced if one notices Profile # 5 is slightly under Profile # 6 near the tip. These two wick thickness profiles are nearly the same between x=0 m and x=0.15 m where Profile # 6 is slightly higher than Profile # 5. Between x=0.15 m and x=0.60 m Profile # 5's wick thickness is

significantly higher resulting in 30% more wick volume in comparison to Profile # 6.

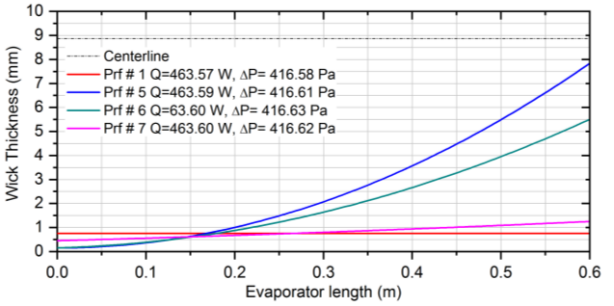

Figure 11. Concave up, increasing wick profiles over evaporator.

Concave down, increasing wick profiles, Figure 12, has lower thickness at evaporator end, x=0.6 m, in comparison to linear increasing and concave up, increasing wick profiles. For the concave down case, the higher the slope at x=0 m, the less the wick thickness at x=0.6 m is, if heat transfer rate remains equal to that of the reference uniform wick profile.

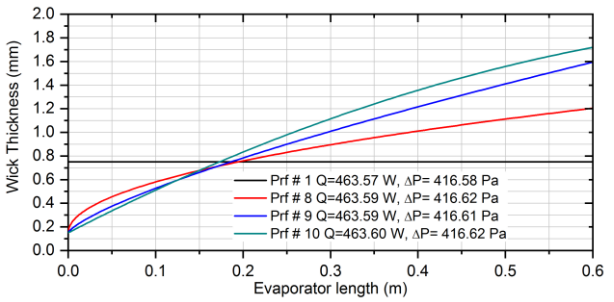

Figure 12. Concave down, increasing wick profiles over evaporator.

Effect of Pressure Loss and Temperature Difference on Heat Transfer Rate

According to Eqs. (29) and (32) heat transfer rate and heat flux are proportional to the square root of pressure loss, ΔP, and temperature difference, ΔT, along and across the wick, respectively. Heat flux given by Eq. (32) as a function of ΔP/L and ΔT/L is plotted in Figure 13 for various thermo-physical group values, "C". An evaporator with a specified value of "C" operates on the relevant surface drawn in Figure 13, whether or not it operates at the design or an off-design, e.g. at a lower temperature difference or heat flux, point. This is because if actual heat flux is lower than the design-point value, fluid flow thus pressure loss reduces and the operating condition stays on the specified surface.

Figure 13 is applicable for uniform and non-uniform evaporator and condenser wick profiles. In case of uniform wick profile heat flux can be expressed as:

$$q'' = k_{eff}\frac{\Delta T}{t} \tag{47}$$

By combining Eqs. (32) and (47)

$$k_{eff}\frac{\Delta T}{t} = C\sqrt{\frac{\Delta P}{L}\times\frac{\Delta T}{L}} \tag{48}$$

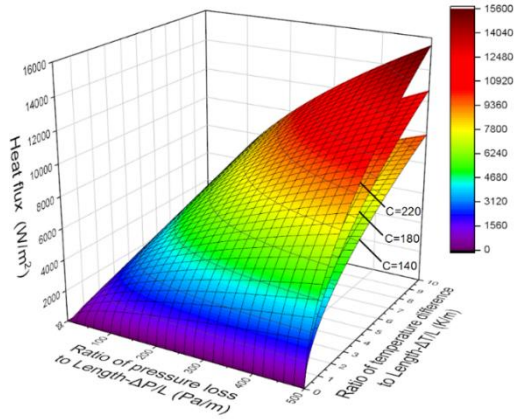

Figure 13. Heat flux as a function of ΔP/L and ΔT/L for various thermo-physical group values, "C".

Equation (48) can be simplified as follows, to obtain an equation for dimensionless wick thickness, t/L, in terms of ΔT/L and ΔP/L

$$C_1 = \frac{C}{k_{eff}} = \sqrt{\frac{2\rho_l K h_{fg}}{\mu_l k_{eff}}} \tag{49}$$

$$\frac{t}{L} = \frac{1}{C_1}\frac{\sqrt{\Delta T/L}}{\sqrt{\Delta P/L}} \tag{50}$$

Dimensionless wick thickness t/L as a function of ΔP/L and ΔT/L is plotted in Figure 14 for various thermo-physical group values, "C_1". Given a specified pressure loss and temperature difference for an evaporator or condenser with uniform wick profile; wick thickness, heat flux and heat transfer rate can be calculated by using Figure 13 and Figure 14. In case of an over designed heat pipe actual temperature difference, heat transfer rate and pressure loss is lower than those at the design point. Pressure loss for an operating condition can be found for a given wick thickness and actual temperature difference using Figure 14. Using the found operating pressure loss and the temperature difference, heat flux and thus heat transfer rate can be calculated from Figure 13.

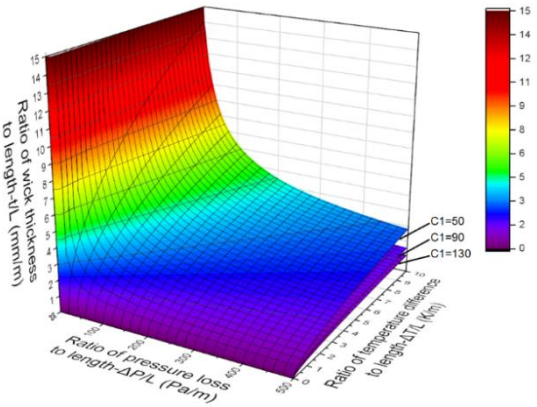

Figure 14. Ratio of wick thickness to length for various thermo-physical group values.

For a wick of 8.65 mm outer radius, heat transfer rate is plotted as a function of pressure loss and temperature difference in Figure 15, where C is 179.3 according to the parameters given in Table 1. It can be concluded that as the pressure loss raises heat transfer rate increases for a given temperature difference. Similarly, as the temperature difference increases, so does the heat transfer rate for a given pressure loss.

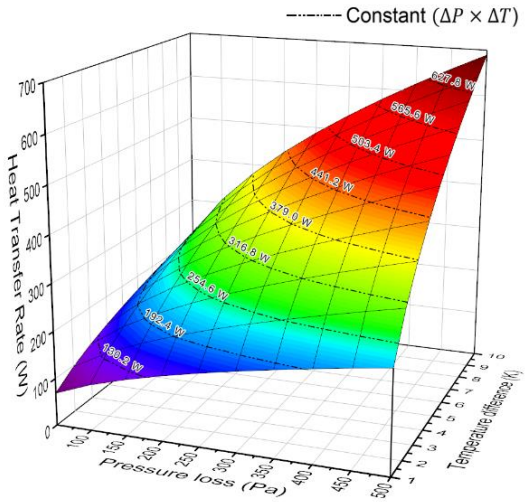

Figure 15. Change of evaporator heat transfer rate with pressure loss and temperature difference.

There exist a hidden variable in Figure 15 which is the wick thickness. Wick thickness should be increased to keep pressure loss along the wick constant if the temperature difference increases as a consequence of increased heat transfer rate and thus the flow rate. Uniform evaporator wick thickness values corresponding to heat transfer rates presented in Figure 15 over the same range of pressure loss and temperature difference values are plotted in Figure 16.

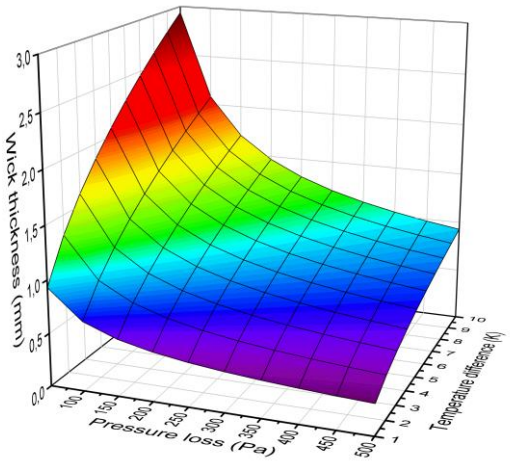

Figure 16. Change of evaporator wick thickness with pressure loss and temperature difference.

1-D Analysis of Flow and Heat Transfer for a Heat Pipe

Analysis of different wick profiles for heat transfer, pressure loss and mass over evaporator and condenser results in a uniform profile as optimal solution. It is also noted that lower the evaporator and condenser wick thickness the higher the heat transfer rate. These insights together with analysis of r_v/r in adiabatic zone for reduced pressure loss leads to two types of designs shown in Figure 17. Increasing adiabatic zone wick thickness up to a critical value of r_v/r results in lower pressure loss as shown in Figure 7, thus higher heat transfer rate at capillary limit. However, it also results in increased vapor pressure loss at the adiabatic zone causing an increase in vapor temperature drop which in turn has a decreasing effect on the heat transfer rate. For this reason, consideration of the entire wick and vapor in a heat pipe including the evaporator, adiabatic zone and the condenser is necessary to apply the findings.

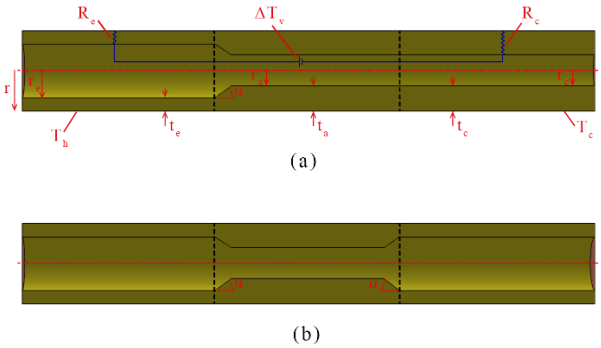

Figure 17. Suggested wick profiles for a heat pipe (a: $t_e < t_a = t_c$, b: $t_e = t_c < t_a$).

To investigate overall wick and vapor system a 1-D model is built which consists of two radial resistances and a potential difference to represent vapor temperature drop in axial direction as shown in Figure 17. Axial heat transfer through the wick is neglected since it is very low in comparison to radial heat transfer rate. Radial thermal resistances of evaporator, R_e, and condenser, R_c, which are obtained from Equations (4) and (40) for uniform wick thickness are

$$R_e = \frac{t_e}{k_{eff} 2\pi r L_e} \tag{51}$$

$$R_c = \frac{t_c}{k_{eff} 2\pi r L_c} \tag{52}$$

Axial vapor temperature drop, ΔT_v, i.e. potential difference in Figure 17 is related to vapor pressure loss since vapor at evaporator and condenser are both saturated at different pressures the difference of which drives the vapor flow. Vapor temperature drop is found using saturation data in thermodynamic tables. Then, heat transfer rate is calculated as follows:

$$Q = \frac{T_h - T_c - \Delta T_v}{R_e + R_c} \tag{53}$$

Liquid and vapor pressure losses in evaporator, adiabatic zone and condenser are calculated by Equations (45) and (46) where adiabatic zone length, L_a, is replaced by evaporator and condenser effective lengths, $L_{eff,e}$, and $L_{eff,c}$, respectively, for evaporator and condenser, which are defined as follows (Zohuri, 2016):

$$L_{eff,e} = \frac{L_e}{2} \quad (54)$$

$$L_{eff,c} = \frac{L_c}{2} \quad (55)$$

If turbulence occurs at any region in the vapor core, pressure loss is calculated by turbulent formulation otherwise laminar approach is applied. The location of laminar to turbulent transition is determined if turbulent flow exists in evaporator due to increased mass flow rate caused by evaporation and thus vapor speed based on Reynolds number criterion (Re > 2300). Same method is applied to the condenser to determine the location of turbulent to laminar transition due to condensation.

Change of wick thickness along the transition regions between evaporator and adiabatic zone and adiabatic zone and condenser is also of scientific interest. In this study, linear wick thickness profile for both transition regions (gradual contraction and expansion) is assumed with α=20°. Local vapor pressure losses due to gradual expansion and contraction are calculated by the semi-empirical formulas from the literature (Crane, 2009; Idelchik, 1994).

In the analyses capillary limit is also considered. For circulation of working fluid, capillary pressure difference, ΔP_{cap}, should be higher than the sum of the liquid pressure loss, ΔP_l, and vapor pressure loss, ΔP_v.

$$\Delta P_{cap} \geq \Delta P_l + \Delta P_v \quad (56)$$

Capillary pressure difference is calculated by Young-Laplace equation as follows:

$$\Delta P_{cap} = \frac{2\sigma}{r_{cap}} \quad (57)$$

Results for Overall Heat Pipe Wick

Using the developed 1-D model for transport phenomena at the wick and vapor, effect of wick thicknesses of evaporator, adiabatic zone and condenser on heat transfer and capillary limit are investigated parametrically. Wick parameters, r, r_{cap}, φ, K, which are kept constant in case studies are given in Table 1. Evaporator, adiabatic zone and condenser lengths are kept equal to each other for convenience as 200 mm. In the analysis, temperature difference, which is the driving potential for heat transfer, between evaporator and condenser wick outer surfaces, T_h-T_c, is kept constant at 20°C, where T_c=25°C.

Under the constraint of constant total, i.e. sum of evaporator, adiabatic zone and condenser, wick volume, and therefore weight, effect of wick thicknesses on heat transfer rate and overall pressure loss are studied for the case depicted in Figure 17 (a) and results are presented in Figure 18. Similarly, under the constraint of constant total wick volume, the design shown in Figure 17 (b) is studied by increasing adiabatic zone wick thickness and results are given in Figure 19. In both cases heat transfer rate and overall pressure loss increases as wick is thickened in the adiabatic zone. However in case of Figure 17 (a) evaporator wick thickness reduces more rapidly than the case presented in Figure 17 (b) to compensate for increased adiabatic zone and condenser wick volumes. This fact results in a rapid increase of overall pressure loss and capillary limit is reached at 349 W, as opposed to gradual increase of overall pressure loss thus higher heat transfer rate which is 742 W in case of Figure 17 (b).

When the performance of the two designs are evaluated by removing the constant overall wick volume constraint following results are obtained. In Figure 20, heat transfer rate is plotted for the case presented in Figure 17 (a) where adiabatic zone and condenser wick thicknesses are equal to each other and higher than that of the evaporator. Increasing adiabatic zone and condenser wick thicknesses up to a certain value enhances heat transfer rate at capillary limit up to 620 W, beyond which heat transfer deteriorates, while it is 583 W in case of uniform wick thickness throughout the heat pipe.

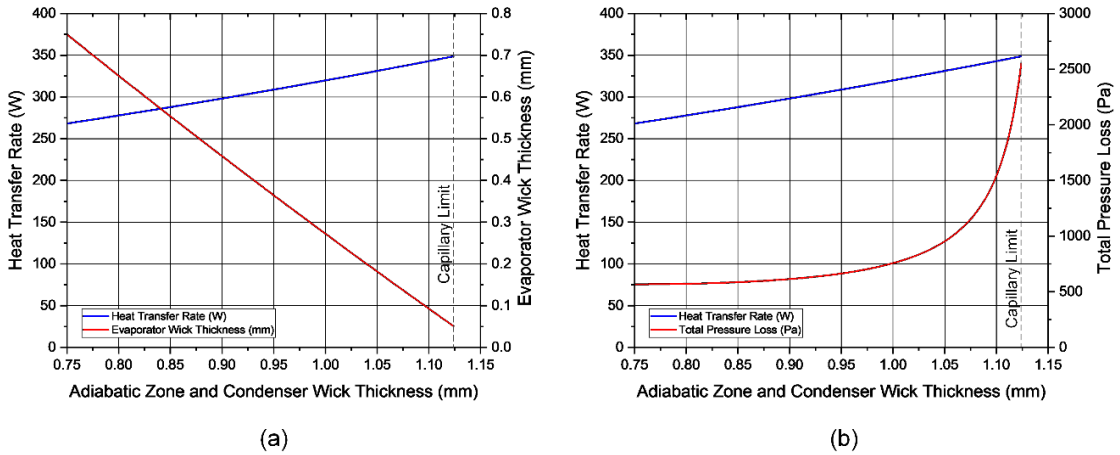

Figure 18. Heat transfer rate with evaporator wick thickness (a) and overall pressure loss (b) as functions of t_a=t_c under constant wick volume constraint for the design shown in Figure 17 (a).

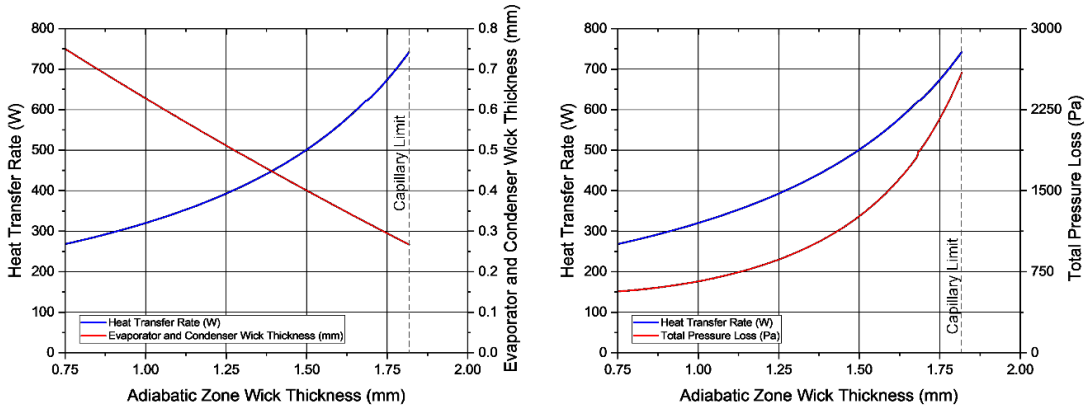

Figure 19. Heat transfer rate with evaporator and condenser wick thickness (a) and overall pressure loss (b) as functions of t_a under constant wick volume constraint for the design shown in Figure 17 (b).

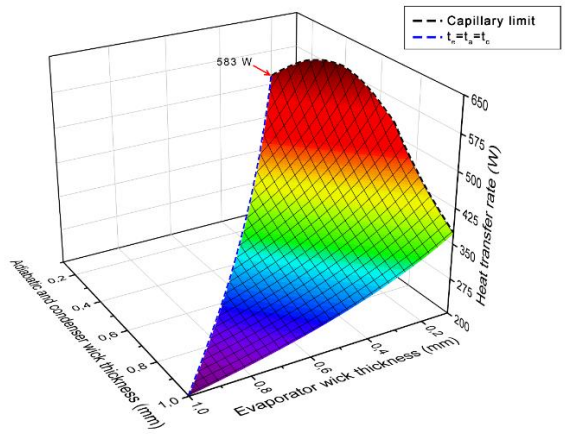

Figure 20. Change of heat transfer rate by wick thicknesses (t_a=t_c).

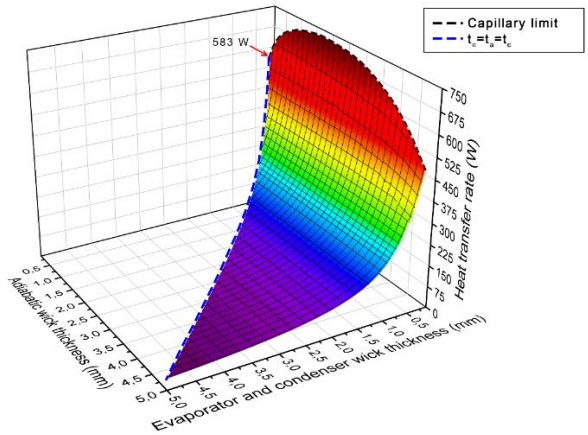

Figure 21. Change of heat transfer rate by wick thicknesses (t_e=t_c).

In Figure 21, evaporator and condenser wick thicknesses kept equal to each other and lower than adiabatic zone wick thickness as shown in Figure 17 (b). Decreasing evaporator and condenser wick thickness increases heat transfer rate rapidly. As stated before, for uniform wick thickness throughout the heat pipe, capillary limit is 583 W. Increasing adiabatic zone wick thickness up to a certain value results in increased capillary limit which reaches 744 W, thereafter it deteriorates. Increase of capillary limit with increasing adiabatic zone wick thickness is due to resulting lower pressure loss in the adiabatic zone which allows higher pressure loss thus lower wick thickness and consequently increased heat transfer rate in evaporator and condenser.

At capillary limit, evaporator and condenser wick thickness and heat transfer rate as functions of adiabatic zone wick thickness are plotted in Figure 22 (a). Increasing adiabatic zone wick thickness above approximately 2 mm decreases maximum heat transfer rate which is due to increased vapor temperature drop as a result of increased vapor pressure loss along the adiabatic zone. Also plotted at the capillary limit is total volume of the wick, Figure 22 (b). As seen from the figure, total wick weight increases as adiabatic zone wick thickness increases. On the other hand, heat transfer rate increases, rapidly between 0.36 mm to 1 mm, at a moderate rate between 1 mm to 1.5 mm and very slowly between 1.5 mm to 2 mm interval of the adiabatic zone wick thickness. This result is significantly important, especially for weight critical applications, since increase of weight has high positive impact on heat transfer rate up to a certain value of adiabatic zone wick thickness. Further increase of weight up to a critical value for which peak value of heat transfer is achieved enhances heat transfer at a reduced rate. Beyond the critical value of weight heat transfer deteriorates at increasing rates as the wick weight is further increased.

As seen from Figure 20 and Figure 21, increasing only adiabatic region wick thickness while lowering that of evaporator and condenser facilitates higher heat transfer rate at capillary limit in comparison to increasing the adiabatic zone and condenser wick thickness while lowering the evaporator wick thickness. This is because of heat transfer rate being inversely proportional to evaporator and condenser wick thicknesses since heat is primarily transferred by conduction in radial direction there.

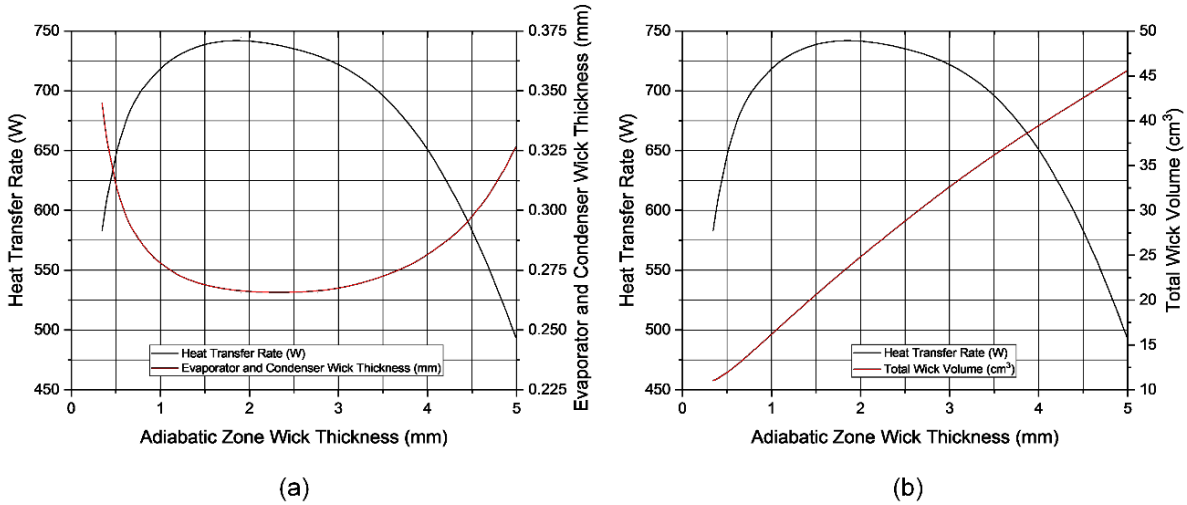

Figure 22. Heat transfer rate, wick thicknesses (a) and total wick volume (b) as a function of adiabatic zone wick thickness at capillary limit.

Lower liquid pressure loss could be obtained for the case in Figure 17 (a) due to higher cross-sectional area of the condenser wick as compared to case in Figure 17 (b). This design results in reduced pressure loss in the adiabatic zone and condenser, while it increases in the evaporator. On the other hand, resistance to radial heat transfer decreases at the evaporator and increases at the condenser. Decrease of radial thermal resistance of the evaporator is higher than increase of that of the condenser so that heat transfer rate is higher as compared to uniform wick thickness case.

Another discussion is real-life application of proposed wick designs. First discussion is the production method for the proposed optimal wick profiles in Figure 17. Normally mono-porous sintered wicks are produced by inserting a rod inside the copper tube, Figure 23 (a), and filling the empty space between the rod and copper tube wall by copper powder. After sintering the copper powder the rod is pulled out leaving the space for vapor flow. However suggested wick profile in Figure 17 (b) does not allow for a rod to be pulled out so it is suggested to use two rods as in Figure 23 (c). One of the rods are inserted from the bottom and another one is inserted from the top side. Then, copper powder is filled from top side and sintered. After the sintering procedure rods are being pulled out from top and bottom avoiding undercut. However by keeping the adiabatic and condenser section wick thicknesses equal, it is possible to produce the wick with a single rod as seen in Figure 23 (b). In this case, heat pipe performance is enhanced without changing the classical heat pipe production method.

In the literature few studies, e.g. (Zohuri, 2016), on variable thickness wicks exist which are aimed at managing non-uniform heat flux at evaporator. Full wetting of variable thickness wick is possible for heat pipes for which axial length is much bigger than pipe radius. For such heat pipes axial pressure loss is much bigger than that across the wick. Typical capillary pumping capacity of heat pipes are quite high so that full wetting in radial direction is guaranteed.

In the literature, variable thickness wick is proposed for thermal management of evaporators subject to non-uniform heating (Zohuri, 2016).

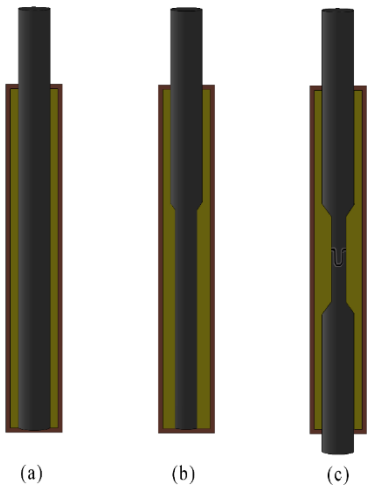

Figure 23. Single rod (a, b) and suggested two rod (c) production methods.

CONCLUSIONS

In this study, first, one-dimensional thermo-fluid model of the transport phenomena in the wick of the evaporator of a heat pipe is developed analytically to study the effect of longitudinal wick profiles on heat pipe performance. Based on the developed model, an analytical relation between pressure loss along and temperature difference across the wick of the evaporator of a heat pipe is derived by one-dimensional analyses based on Darcy's Law of pressure loss of liquid flow in a porous medium and Fourier's Law of Heat Conduction, see Equation (17). In this expression both thermo-fluid properties of the working fluid and porous wick and integral of the reciprocal of thickness profile of the wick along the evaporator appear. Furthermore, heat transfer rate is expressed in terms of outer radius and permeability of the wick, thermo-fluid properties of the working fluid, liquid pressure loss along the wick and temperature difference

across the wick, for any wick thickness profile, see Equation (18). It is found that same pressure loss and heat transfer rate can be obtained with different evaporator wick profiles. It is shown that the ratio of the evaporator heat transfer rate to the square root of the liquid axial pressure loss in the wick of the evaporator times the temperature difference across the evaporator wick is constant for a chosen working fluid and wick micro-structure, see Equation (29).

Secondly, an isoperimetric problem of calculus of variations is solved to find the evaporator wick thickness profile that minimizes evaporator wick volume, thus weight, under the constraints of fixed heat transfer rate and admissible wick thickness profiles satisfying a chosen liquid pressure loss along the wick, see Equation (34), which results in a uniform wick thickness along the evaporator. Uniform wick thickness as given by Equation (37) is expressed in terms of the length of the evaporator, outer radius and permeability of the wick, thermo-fluid properties of the working fluid, as well as the liquid pressure and temperature differences along and across the evaporator wick.

Then, the thermo-fluid model and the results of the optimization problem are extended to the condenser section of the heat pipe. As in the case of evaporator, condenser heat transfer rate can be calculated in term of outer radius and permeability of the wick, thermo-fluid properties of the working fluid, and liquid pressure and temperature differences along and across the condenser wick, respectively, for any wick thickness profile. For a given heat transfer rate, among the wick thickness profiles that satisfy a specified liquid pressure drop along the wick of the condenser, as in the case of evaporator, minimum material use is achieved by keeping the wick thickness uniform, which can be calculated by Equation (37).

Finally, the uniform wick thickness that minimizes the sum of the pressure losses along the wick and the central vapor column of the adiabatic zone of the heat pipe is calculated based on Darcy's Law for liquid flow in porous wick and Poiseuille-Hagen and Darcy-Weisbach formulas for laminar and turbulent vapor flows, respectively. It is concluded that wick thickness in evaporator and condenser may need to be less than that of the adiabatic zone in order to enhance heat transfer rate while keeping sum of the liquid and vapor phase pressure losses in the adiabatic zone at minimum value.

Under the constraint of overall pressure loss in heat pipe cycle which is imposed by capillary head, the wick thicknesses of evaporator, adiabatic zone and condenser should be selected in such a way that heat transfer rate is maximized. Therefore, two novel piecewise uniform wick thickness profiles, one with bigger wick thickness in adiabatic zone as compared to that of the evaporator and condenser, and the other with common wick thickness of the adiabatic zone and condenser being bigger than that of the evaporator are proposed to realize the target mentioned above.

Coupled flow and thermal analyses in the wick and vapor core showed that for a conventional heat pipe, i.e. uniform wick thickness throughout the heat pipe, of specified length, radius and wick porous structure operating at a specified temperature difference heat transfer rate is 268 W. Under constant total wick volume constraint, when adiabatic zone and condenser wick thicknesses are increased by keeping them equal to each other and evaporator wick thickness is lowered, heat transfer rate is found to increase up to 349 W when capillary limit is reached. On the other hand, under the same constraint, if evaporator and condenser wick thicknesses are equal to each other and adiabatic zone wick thickness is higher, calculations show that heat transfer rate can be increased up to 742 W when capillary limit is reached.

In case of the design where adiabatic zone wick thickness is higher than that of evaporator and condenser, when the constant wick volume constraint is removed heat transfer rate can be increased up to 27.6% at capillary limit which is achieved for total wick volume increase of 136% in comparison to conventional heat pipe. On the other hand, if adiabatic region and condenser wick thicknesses are equal and higher than that of evaporator heat transfer rate increases up to 6.3% at capillary limit where total wick volume increases 6.9%.

Since developed model is kept simple to make it analytically solvable, future work may focus on evaluation of the performance of suggested designs by more-sophisticated multi-dimensional models such as an axisymmetric thermo-fluid model incorporating pressure losses in radial direction, pressure jump at liquid vapor interface due to capillarity, interfacial resistance to heat transfer and axial heat transfer in the wick.

It is well known that sum of the pressure losses in the heat pipe should be less than the capillary head. Designs suggested in this study modify distribution of pressure loss among various wick zones to enhance heat transfer rate at capillary limit. However, in the analyses, evaporator, condenser and adiabatic zone lengths are kept equal to each other which may not be the case in real applications. Also wick thicknesses in the analyses changed in pairs, i.e. wick thickness of the condenser is kept equal to that of the adiabatic zone, or wick thickness of the condenser is kept equal to that of evaporator, but the influence of different wick thickness for each zone on the performance is not evaluated in this study. Therefore, it is necessary to derive optimal ratios of evaporator, adiabatic zone and condenser wick thicknesses for a heat pipe with various lengths of the three zones.

ACKNOWLEDGEMENTS

Authors gratefully acknowledge suggestions and support of Dr. İsmail Teke of Yıldız Technical University, Istanbul and Dr. İlyas Kandemir of Gebze Technical University, Gebze-Kocaeli. Authors also deeply appreciate assistance of Muhammed Said Gündoğan of Bilkent University, Ankara.

REFERENCES

Crane Co., 2009, Flow of Fluids Through Valves, Fittings and Pipe, Technical Paper No. 410.

Deng D., Liang D., Tang Y., Peng J., Han X. and Pan M., 2013, Evaluation of capillary performance of sintered porous wicks for loop heat pipe, Exp. Therm. Fluid Sciences, 50, 1-9.

El-Genk M. S. and Huang L., 1993, An experimental investigation of the transient response of a water heat pipe, Int. J. Heat Mass Transfer, 36, 3823-3830.

Gelfand I. M. and Fomin S. V., 1963, Calculus of variations, Prentice-Hall.

Hong, F.J., Cheng P., Wu H.Y. and Sun Z., 2013, Evaporation/boiling heat transfer on capillary feed copper particle sintered porous wick at reduced pressure, Int. J. Heat Mass Transfer, 63, 389–400.

Huang Y. and Chen Q., 2017 ,A numerical model for transient simulation of porous wicked heat pipes by lattice Boltzmann method, Int. J. Heat Mass Transfer, 105, 270–278.

Idelchik I. E., 1994, Handbook of Hydraulic Resistance, CRC Begell House.

Kaya T., Goldak J., 2007, Three-dimensional numerical analysis of heat and mass transfer in heat pipes, Heat Mass Transfer, 43, 775–785.

Kiseev V.M., Vlassov V.V. and Muraoka I., 2010, Optimization of capillary structures for inverted meniscus evaporators of loop heat pipes and heat switches, Int. J. Heat Mass Transfer, 53, 2143-2148.

Lemons D.S., 1997, Perfect Form: Variational Principles, Methods and Applications in Elementary Physics, Princeton University Press.

Lin K.T. and Wong S.C., 2013, Performance degradation of flattened heat pipes, Appl. Therm. Engineering, 50, 46–54.

Mwaba M.G., Huang X. and Gu J., 2006, Influence of wick characteristics on heat pipe performance, Int. J. Energy Research, 30, 489–499.

Nishikawara M. and Nagano H., 2017, Optimization of wick shape in a loop heat pipe for high heat transfer, Int. J. Heat Mass Transfer, 104, 1083-1089.

Ranjan R., Murthy J.Y. and Garimella S.V., 2009, Analysis of the wicking and thin-film evaporation characteristics of microstructures, J. Heat Transfer, 131, 1–11.

Ranjan R., Murthy J.Y., Garimella S.V. and Vadakkan U., 2011, A numerical model for transport in flat heat pipes considering wick microstructure effects, Int. J. Heat Mass Transfer, 54, 153-168.

Schmalhofer J. and Faghri A., 1992, A study of circumferentially- heated and block- heated heat pipes-l. Experimental analysis and generalized analytical prediction of capillary limits, Int. J. Heat Mass Transfer, 36, 201-212.

Siddiqui A. and Kaya T., 2016, Design and thermal analysis of a segmented single-artery heat pipe, Appl. Therm. Engineering, 96, 652–658.

Tournier J.M. and El-Genk M.S., 1994, A heat pipe transient analysis model, Int. J. Heat Mass Transfer, 37, 753–762.

Wang Q., Hong J. and Y. Yan, 2014, Biomimetic capillary inspired heat pipe wicks, J. Bionic Engineering, 11, 469–480.

Weibel J.A., Garimella S.V. and North M.T., 2010, Characterization of evaporation and boiling from sintered powder wicks fed by capillary action, Int. J. Heat Mass Transfer, 53, 4204–4215.

Wong S.C., Cheng H.S. and Tu C.W., 2017, Visualization experiments on the performance of mesh-wick heat pipes with differing wick wettability, Int. J. Heat Mass Transfer, 114, 1045-1053.

Zhu N. and Vafai K., 1999, Analysis of cylindrical heat pipes incorporating the effects of liquid-vapor coupling and non-Darcian transport - a closed form solution, Int. J. Heat Mass Transfer, 42, 3405–3418.

Zohuri B., 2016, Heat pipe design and technology: Modern applications for practical thermal management (2nd Ed.), Springer.

Zuo Z.J. and Faghri A., 1998, A network thermodynamic analysis of the heat pipe, Int. J. Heat Mass Transfer, 41, 1473–1484.

APPENDIX - CALCULATION OF ADIABATIC ZONE PRESSURE LOSSES FOR VARIOUS WICK PROFILES

If vapor flow is laminar, sum of the pressure losses in vapor and liquid phases, in differential form, can be expressed as

$$dP_a = \frac{C_1}{(r-f(x))^4}dx + \frac{C_2}{[r^2-(r-f(x))^2]}dx \quad (1)$$

If vapor flow is turbulent, sum of the pressure losses in vapor and liquid phases, in differential form, becomes

$$dP_a = \frac{C_3}{(r-f(x))^5}dx + \frac{C_2}{[r^2-(r-f(x))^2]}dx \quad (2)$$

where constants C_1, C_2 and C_3 are defined as follows:

$$C_1 = \frac{8\mu_v \dot{m}}{\pi \rho_v} \quad (3)$$

$$C_2 = \frac{\mu_l \dot{m}}{\pi \rho_l K} \quad (4)$$

$$C_3 = \frac{f\dot{m}^2}{4\pi^2 \rho_v} \quad (5)$$

Vapor column radius is presented as r_v=r-f(x) since different adiabatic zone wick thickness profiles, f(x), are to be considered.

Table 1. Typical water-copper heat pipe parameters for the case studies.

Parameter	Value	Unit
L_a	90	mm
μ_v	1.1x10^{-5}	Pa s
μ_l	4.7x10^{-4}	Pa s
ρ_l	983.2	kg/m^3
ρ_v	0.13	kg/m^3
r	8.65	mm
φ	0.5	%
K	1.5x10^{-9}	m^2
f	0.13	-
$\dot{m}$	0.188	gr/s

Adiabatic zone pressure loss is found by integrating Equations (1) and (2) over the adiabatic zone length.

$$\Delta P_a = \int_0^L \left(\frac{C_1}{(r-f(x))^4} + \frac{C_2}{[r^2-(r-f(x))^2]}\right)dx \quad (6)$$

$$\Delta P_a = \int_0^L \left(\frac{C_3}{(r-f(x))^5} + \frac{C_2}{[r^2-(r-f(x))^2]}\right)dx \quad (7)$$

Values of C_1, C_2 and C_3 are calculated by parameters given in Table 1. Friction factor f in Equation (5) is calculated for Re=3161 which is reached at r_v=3.46 mm. Friction factor is assumed to be constant throughout the adiabatic zone in the following analyses.

Pressure losses calculated by Equation (6) for constant, linearly increasing and linearly decreasing wick thickness profiles under the constraint of constant wick volume are presented in Table 2 for laminar vapor flow. In Figure 1 wick thickness profiles given in Table 2 are plotted.

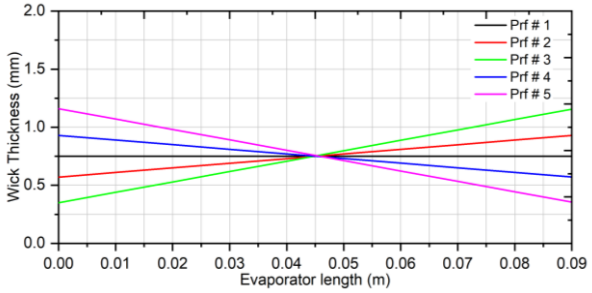

Figure 1. Wick thickness profiles given in Table 2 over adiabatic zone length.

As seen from Table 2 and Table 3, uniform wick thickness results in the lowest pressure drop in comparison to linearly increasing and decreasing wick profiles. Under constant wick volume constraint, pressure losses in both phases increase along with the absolute value of the slope of the wick profile, for both flow regimes.

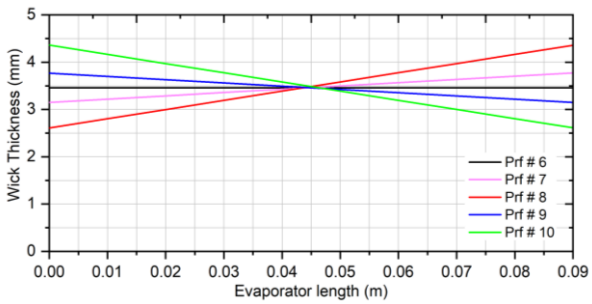

Figure 2. Wick thickness profiles given in Table 3 over adiabatic zone length.

Table 2. For laminar vapor flow, pressure losses for various adiabatic zone wick thickness profiles.

Profile No	Wick profile (mm)	Vapor pressure loss (Pa)	Liquid pressure loss (Pa)	Total pressure loss (Pa)	Wick volume (cm^3)
1	$f(x) = 0.75$	0.927	137.141	138.068	3.51
2	$f(x) = 3.99x + 0.57$	0.928	139.821	140.749	3.51
3	$f(x) = 8.95x + 0.35$	0.936	151.845	152.781	3.51
4	$f(x) = 0.93 - 3.99x$	0.928	139.821	140.749	3.51
5	$f(x) = 1.16 - 8.95x$	0.936	151.845	152.781	3.51

Table 3. For turbulent vapor flow, pressure losses for various adiabatic zone wick thickness profiles.

Profile No	Wick profile (mm)	Vapor pressure loss (Pa)	Liquid pressure loss (Pa)	Total pressure loss (Pa)	Wick volume (cm^3)
6	$f(x) = 3.46$	21.37	35.55	56.92	13.54
7	$f(x) = 6.92x + 3.15$	21.79	35.62	57.41	13.54
8	$f(x) = 19.43x + 2.61$	25.28	35.99	61.27	13.54
9	$f(x) = 3.77 - 6.92x$	21.79	35.62	57.41	13.54
10	$f(x) = 4.36 - 19.43x$	25.28	35.99	61.27	13.54

Mehmed Akif PAKSOY was graduated from Middle East Technical University, Ankara, Turkey in 2012. He received his Masters degree in Mechanical Engineering from Gebze Technical University, Kocaeli, Turkey in 2014. He worked as design and analyses engineer for public and private companies. He is currently working as a senior researcher for The Scientific and Technological Research Council of Turkey. His research interests include heat pipes, computational fluid dynamics, heat transfer and mechanical design.

Salih Özen ÜNVERDİ was graduated from Istanbul Technical University, Istanbul, Turkey in 1982. He received his Ph.D. degree from University of Michigan, Ann Arbor, Michigan, USA in 1990. He is one of the pioneers of the front-tracking method for direct numerical simulations of multi-phase flows. He worked for several global and local automotive companies as design and analyses engineer. He is currently lecturing and researching in Mechanical Engineering Department of Gebze Technical University. His research interests include computational fluid dynamics, heat transfer, thermodynamics and combustion.